



An investigation into directional characteristics of the rocket plane in a tailless configuration

Agnieszka Kwiek¹ · Marcin Figat¹

Received: 28 February 2022 / Revised: 20 July 2022 / Accepted: 30 July 2022 / Published online: 29 August 2022
© The Author(s) 2022

Abstract

This paper embraces result of wind tunnel tests of a rocket plane designed to space tourism application. The rocket plane is designed in a tailless configuration with a leading edge extension (LEX) and side plates on the wing's tip which work as all moving tail. Usually for such a concept of control, movable surfaces are position in a horizontal direction while in the considered concept there is no classical rudder, and the movable surfaces are mounted with a significant dihedral angle. The research was carried out in the subsonic closed circuit wind tunnel with an open test section. Moreover, MGAERO and PANUKL package were used for numerical computations. The first research question is to investigate how the configuration of the side plate affects the directional stability of the rocket plane. The second aim is to study the efficiency of the side plates deflected like an all moving tail for both low and high angles of attack. As a result of this investigation, the directional stability derivatives and the control derivatives were obtained. Finally, the experimental results were compared with numerical outcomes to establish does software with no full flow model can be applicable for design an aircraft with all moving tail in case of low of angles of attack.

Keywords Wind tunnel tests · Directional aerodynamic characteristics · Directional control surface efficiency · Rocket plane · Space tourism

Abbreviations

α	Angle of attack (AoA)
β	Side slip angle
$\frac{\partial C_Y}{\partial \beta}$	Derivative of side force coefficient in respect to side slip angle
$\frac{\partial C_n}{\partial \beta}$	Derivative of yaw moment coefficient in respect to side slip angle
δ_R	Angle of both side plates deflection (symmetrical deflection)
δ_{RR}	Angle of right side plate deflection
δ_{RL}	Angle of left side plate deflection
Θ_d	Yaw angle of lower side plate
Θ_u	Yaw angle of upper side plate
λ_d	Taper ratio of lower side plate

λ_u	Taper ratio of upper side plate
C_D	Drag coefficient
C_L	Lift coefficient
C_{MY}	Pitching moment coefficient
C_n	Yaw moment coefficient
C_Y	Side force coefficient
MAC	Mean aerodynamic chord
TL	Trend line
Re	Reynolds number

1 Introduction

The suborbital flights can be a cheaper alternative for orbital space flights. For a such kind of flight, multiple applications can be listed [1] and [2], including educational purposes and improving products' TRL level. While manned suborbital flights can be an opportunity for people who were not trained as professional astronauts and would like to visit the outer space by paying relatively low price compared to the orbital space flights. The booster for the development of the concept of reusable suborbital vehicles to commercial space tourist flights was the Ansary X-Prize competition that was won in

✉ Agnieszka Kwiek
agnieszka.kwiek@pw.edu.pl

Marcin Figat
marcin.figat@pw.edu.pl

¹ Aircraft Design Division, The Institute of Aeronautics and Applied Mechanics, Warsaw University of Technology, Nowowiejska 24, 00-665 Warsaw, Poland

2004 by the Tier One Project (Space Ship One rocket plane and White Knight mother plane). Next, the race of designing a vehicle that is going to use for commercial operations begun. The first suborbital flight with a customer on-board took place on the 20th of July 2021. The second commercial flight was on the 13th of October 2021. Both flights were above the Karman line (100 km above the sea level) and performed by the New Shepard (Blue Origin) spacecraft. The second company which is a major player in suborbital tourist flights race is the Virgin Galactic. They performed a fully crewed flight above 50 miles on the 11th of July 2021 using the Virgin Galactic VSS Unity rocket plane, with the founder Richard Branson and the company vice president Sirisha Bandla on-board. Also, the Virgin Galactic's license issued by the FAA for commercial space flights was expanded to fly customers. Those events are indicating that the era of suborbital manned commercial flights just begun.

An alternative application of the suborbital flights is a point to point transportation. Studies on both spaceport and vehicles can be found in [3–5] and [6]

The researchers from the Warsaw University of Technology were inspired by the Ansary X-Prize competition and begun to work on their own concept of vehicle for manned suborbital tourism flights [7, 8]. The MAS (Modular Airplane System) project consists of two airplanes—a mother plane and a rocket plane (see Fig. 1). Individually each of those vehicles is designed as a tailless aircraft while connected together creating a conventional aircraft. The rocket plane's wing is utilized as an empennage of the whole system. To enhance the aerodynamic force generated by the rocket plane and increase the critical angle of attack, the leading edge extensions (LEX) was applied [9] and [10]. Another feature that distinguishes the proposed project from the Tier One project are side plates attached to the rocket plane's wing tips which working as the all moving tail (see Fig. 4). The rocket plane can take two passengers and one pilot on-board, the crew compartment which is located in the nose (Fig. 2). While the hybrid rocket engine is placed in the aft section. The shape of the fuselage was design to accommodate both passengers and all necessary systems including the hybrid rocket engine. The weight ratio of the rocket

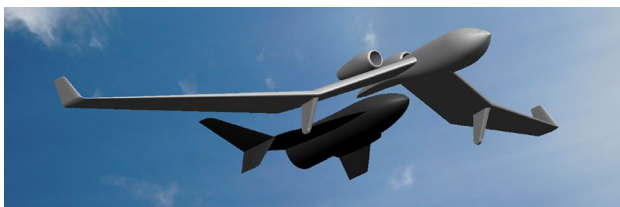


Fig. 1 The concept of MAS (Rocket plane – dark grey; Mother plane – light grey). Both airplanes designed in tailless configuration while in coupled configuration the rocket plane works as empennage

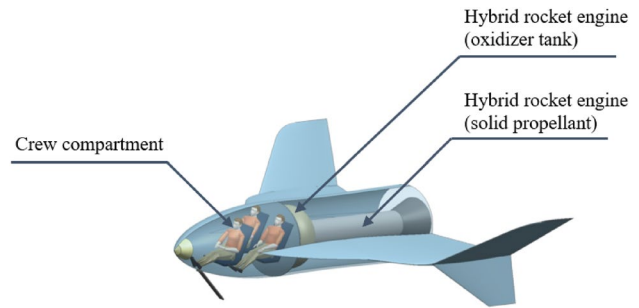


Fig. 2 Rocket plane's inside layout

plane take-off weight and the propellant weight is equal to 2.46. The carrier is also designed as a tailless aircraft, for operations required two-man crew. The aircraft is propelled by two jet engines, of the total thrust is equal to 28.46 kN. The take-off weight of the standalone carrier is 5615 kg. The carrier pitch and roll motion can be control by the elevons while the yaw motion can be controlled by the rudder placed on the winglets.

The assumed mission profile for MAS is presented in Fig. 3. The rocket plane is lifted by the carrier up to 15 km, where the vehicles separate. The study into g-load acting on passengers during the separation process is presented in [14] and concluded that to achieve the lowest possible g-load the separation process should be performed with speed of 100 m/s. But the separation with speed of 155 m/s still gives the g-load that is lower than FAA recommendation and helps to achieve the necessary speed at the end of the climb phase. Next, the rocket plane's engine is igniting, and the rocket plane begins climbing. At the altitude of 67 kms the engine is shut down and the rocket plane begins ballistic flight. The rocket plane achieves altitude higher than 100 km. Then the side plates and elevons are deflected to prepare the rocket plane for return flight configuration which allows on flight at high AoA to engage the lift vortex phenomenon in the aerobraking. The next phase is the transition from high AoA to low AoA. The last element of the rocket plane's mission is landing.

The concept of the rocket plane assumes the use of all moving tail to both the directional and longitudinal control (see Fig. 4). It was assumed that it should satisfy the pitching and yawing moment control for both the low and high Mach numbers. Results of previous research of both the MAS project and the rocket plane are included in [7, 8, 11, 12, 13] While the result of numerical simulation and flight camping conducted to test the rocket plane response to control in longitudinal channel is presented in [14].

The next stage of the project is more detailed simulation of the rocket plane trajectory. To solve this problem a reliable results of control characteristics are necessary. This paper is emphasized on directional characteristics and

Fig. 3 MAS mission profile

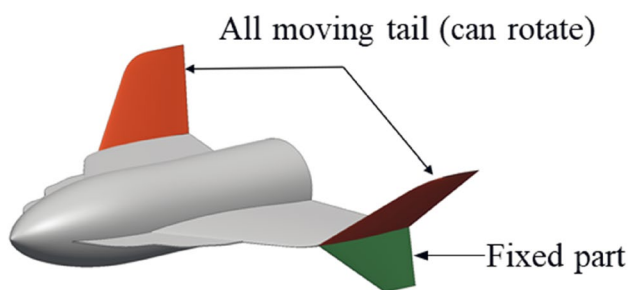
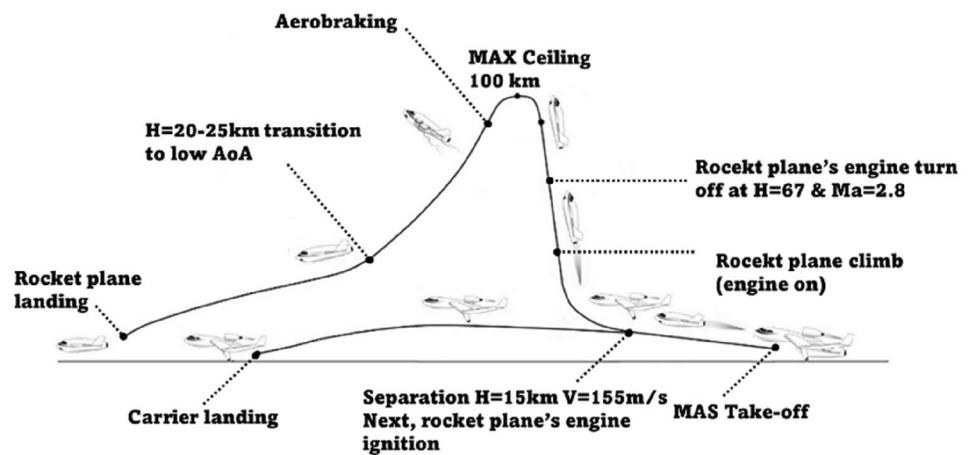


Fig. 4 The concept of control, upper plates could rotate while the bottom one was fixed

method for a yaw control of the rocket plane. One of the goals was to investigate the idea of using this unconventional configuration in control of the yaw motion. Because this is a preliminary study it was decided that before it can be tested in conditions that can correspond to a specific point on the trajectory, a smaller subsonic wind tunnel with a quite low maximum speed (40 m/s) is going to be use first. Because the generation of the vortex lift does not depend on Reynolds number [25] then conducting the experiment for condition of Re bigger than critical Re allow to address another challenge which is the confirmation that the MGAERO software is a sufficient tool to be use in prediction of aerodynamic characteristics of the vehicle with strong aerodynamic coupling. The major factor that causing this coupling is the strong vortex structure due to the LEX presents. Also, investigation how useful for such an unconventional configuration can be a potential flow software, in case of low AoA. Then in the future, the numerical software like MGAERO could be use in more accurate estimation of the flight condition during the mission and this information can be utilized to plan next more complex wind tunnel tests campaign.

The experimental results which are presented in this paper belong to a bigger wind tunnel tests campaign, for example, experimental and numerical study into the impact

of the rocket plane configuration on the longitudinal characteristics can be found in [15] including plots of lift, drag, and pitching moment coefficient.

The concept of the all moving tail is not a new idea but due to a primarily military applications of a such design widely available literature in this area is limited. Especially there is a lack of papers about the design guidelines for this kind of control surface arrangement and its effectiveness. Examples of aircraft which are equipped with this type of the control surfaces are F14, F16, F18, MIG 29, and MIG 35. All those aircrafts using as control surfaces the all moving tail to only control pitch and roll motion while the yaw motion is controlled by a classical rudder. The movable surfaces are position in a horizontal direction while in the considered concept the novel part is that there is no classical rudder, and the movable surfaces are mounted with a significant dihedral (yaw) angle which allows to control both yaw and pitch motion. Such kind of configuration can be very beneficial for aircraft that should has compact design to be more difficult to be detected by a radar. Outcomes of the research into the impact of the side plates dihedral on longitudinal characteristics are presented in [13]. In the literature can be found example of research regarding lateral and directional static stability of tailless vehicle with twin vertical tails [16]. Also, outcomes of the study into the impact of vortex flow on directional characteristics of delta wing with a single and twin vertical tail are presented in [17] and [18].

2 Methodology

In this study, both numerical and experimental methods were used. The numerical outcomes were computed by the MGAERO software and PANUKL package. The first one is a commercial software for aircraft's aerodynamic computations which utilizing the flow model described by Euler's equations [19] and [20]. The limitation of the software is that

a vortex can be simulated but not its breakdown [21]. The considered rocket plane is equipped with the LEX, therefore, a strong vortex structure is expected which is going to affect the efficiency of the side plates. The MGAERO software is using a multigrid scheme to enhance computations efficiency. The numerical model of rocket plane for the MGAERO computations included 7 levels of grids. Both the body grid and multigrid scheme is presented in Fig. 5. All computations were done for precondition equal to 1 and CFL number on each level equal to 4 (default MGAERO set-up). The flow model simulated by the MGAERO software was compressible and inviscid.

The second numerical tool is the PANUKL package [22] which belongs to low order potential method (irrotational, inviscid, and incompressible flow). This software was used for computations of low angles of attack only. The numerical model consists of 6524 elements of the body grids. The numerical tools were used to determine does software with no full flow model can be useful for the design of an aircraft with all moving tail in case of a range of low angles of attack. The PANUKL package using the potential flow and required relatively low amount of

the computation time. The package already proved that it can be successfully applied for design unconventional configurations [23] and [24].

The aim of the experiment was to collect the aircraft aerodynamics characteristics as well as to verify if the numerical results are reliable in terms of the vortex flow simulations. Because the vortex breakdown is independent of the Reynolds number [25], the experiment was carried out in the subsonic wind tunnel for the Reynolds number which was bigger than the critical Reynolds number this is going to ensure that the flow behavior is comparable.

Figure 6 presents example of C_p distribution computed by the PANUKL and MGAERO software. In case of the PANUKL model (picture on the left), the conical shape was added to avoid issue with the flat surface closing the fuselage. But the rocket plane results (coefficients) were computed by sum up all panels excluding the panels on the cone.

Fig. 5 The mesh on the rocket plane and structure of the multi-grid blocks

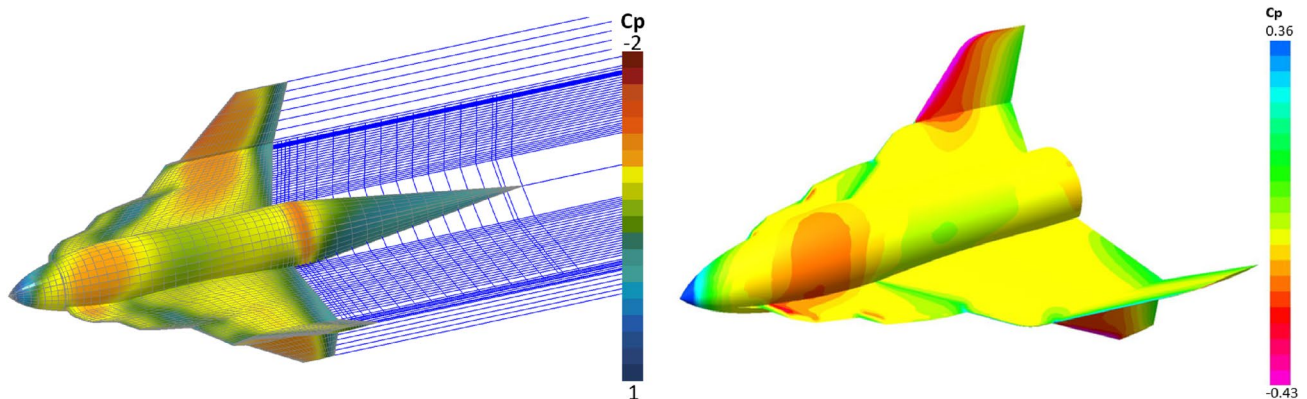
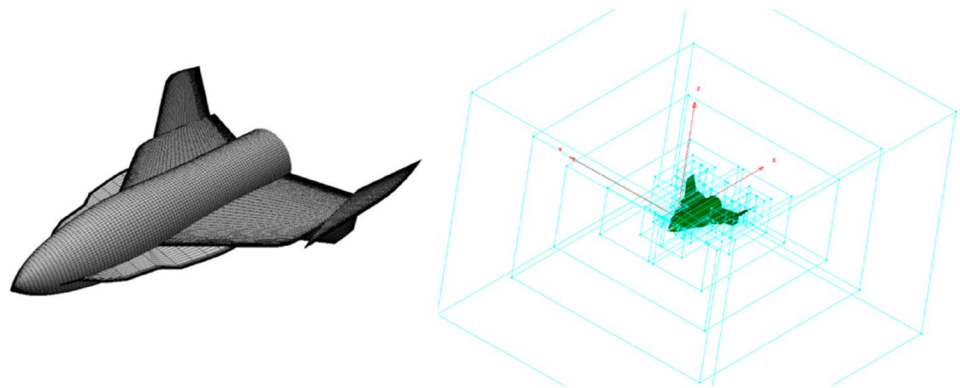


Fig. 6 Example of C_p distribution for $\alpha=0$ deg. and $\beta=5$ deg. computed by PANUKL (picture of the left) and MGAERO (picture on the right)

3 Wind tunnel test

3.1 Experimental model

The 1:15 scale model was built to carry out tests in the wind tunnel (see Fig. 7). The summary of geometrical feature of the wind tunnel model and the full-scale rocket plane is presented in Table 1. The design of the model was planned in a way that the rocket plane’s components can be easily exchanged. The design of the wind tunnel facility allowed for attaching the fuselage as a base element. The fuselage’s shape was the same for all analyzed configurations. While rests of components (wing, LEX, and side plates) can be switched, to ensure that tests of different geometrical configurations are possible. Three different sets of each component were built, the impact of the LEX and wingtip plates on the longitudinal characteristics is presented in [15]. While this paper showing results for a single wing, a single LEX, and two configurations of the side plates only. Each set of the side plates is described by different yaw angles between the upper and lower plate (Θ_u, Θ_d). All sets have the same arm and area of the lower and upper plate. All configurations together with their denotations are presented in Fig. 8.

3.2 Wind tunnel

The subsonic 1.16 m closed-circuit open test section wind tunnel was used to carry out experimental tests. The wind tunnel is located at the Warsaw University of Technology (the Faculty of Power and Aeronautical Engineering) and is equipped with the Witoszyński type balance [27] with a digital data acquisition system. In cases of collecting data for directional characteristics, the set-up of the wind tunnel allowed for measurement of the drag, side force, and yawing moment.

The wind tunnel model was designed as a modular object with exchangeable components. The fuselage geometry was the same for all considered configurations. The wing, LEX,

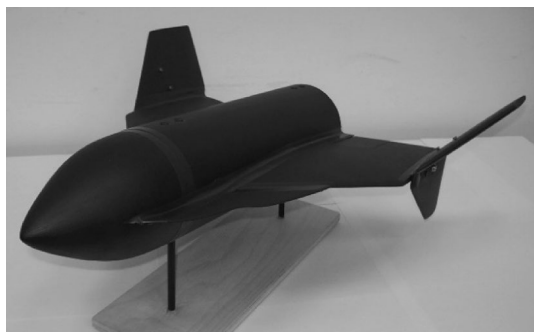


Fig. 7 Experimental model

Table 1 Summary of the rocket plane geometrical dimensions

Parameter name	Full scale rocket plane	Wind tunnel model
Wingspan (without the side plates) [m]	5	0.333
Wing area [m ²]	18.84	0.084
MAC [m]	3.848	0.196

and side plates were separate components, therefore, different geometries of those components could be tested. The rocket plane model was hanged by means of wires which passed through muffs in the fuselage (see Fig. 9). The fuselage was the same for all considered configurations and the attachments of rests of components were designed in a way that any component could be installed without removing the fuselage from the balance. This allows keeping the same model position for all geometrical configurations and ensure that all measurements are done regarding the same reference point. Both the wing and the LEX were attached directly to the fuselage while the side plates were attached to the wing’s tip.

3.3 Test conditions and assumptions

All presented results were measured in the aerodynamic coordinate system at a free stream velocity equal to 40 m/s. The Reynolds number computed based on this speed and the mean aerodynamic chord (MAC) is about $Re = 7 \cdot 10^5$.

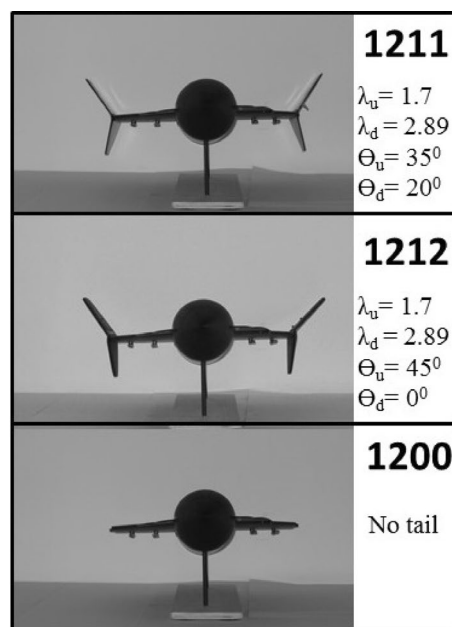


Fig. 8 Configurations of the all moving tail with denotations



Fig. 9 The experimental model hanged in the wind tunnel for the directional cases

All measurements were taken in respect to 21% of the MAC which correspond to one of the rocket plane centers of gravity. Also, the following assumptions for all directional tests were made:

- The positive value of sideslip angle is defined in Fig. 10.
- The positive value of sideslip angle generates a positive side force and yawing moment (see Fig. 10).

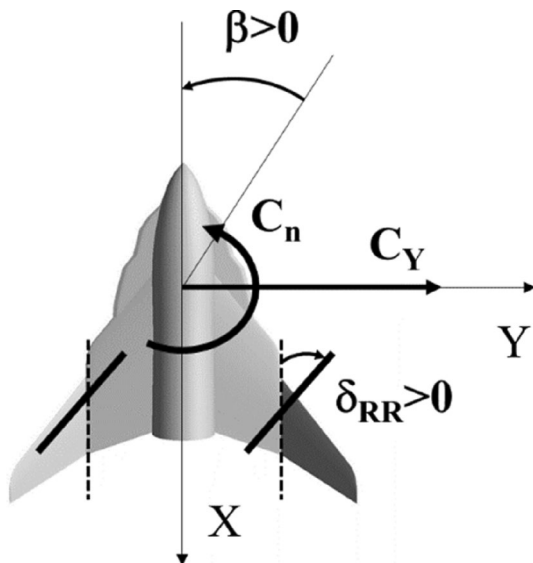


Fig. 10 Force and moment sign convention and positive all moving tail deflection

- The positive value of the all moving tail symmetrical deflection is defined in Fig. 10. The asymmetrical all moving tail deflection occurs when only a single plate (right or left) is deflected.
- The yawing moment coefficient (C_n) is referred to the rocket plane wingspan without the side plates installed on the wing's tips (see Fig. 10).

The directional characteristics were measured within the range of sideslip angle between 0° and $+40^\circ$ and for two angles of attack. Firstly for $\alpha = 0^\circ$ which represents the case of a low angle of attack and then for $\alpha = 27.5^\circ$, just before the stall angle of attack.

4 Results

4.1 Directional aerodynamic characteristics

During the experiment, models with different side plates configurations were examined. Tests were carried out for the model with the side plates in configurations 1211 and 1212 (see Fig. 8). The configuration 1200 which represents the case of the rocket plane without the side plates (Fig. 8) was tested as well to estimate the impact of the side plates on directional characteristics of the complete rocket plane. Moreover, configuration 1212 (see Fig. 8) was chosen to examine the concept of rocket plane directional control by deflecting the upper side plates like the all moving tail. Both symmetrical and asymmetrical deflections were tested. A picture of the model 1212 with a sample symmetrical deflection of control surfaces is presented in Fig. 11.

The first part of the experimental results are measurements for different rocket plane configurations when the angle of attack is equal to $\alpha = 0^\circ$. The plots of the yawing moment coefficient and side force coefficient versus the sideslip angle are presented in Fig. 12. The same types of plots but for the angle of attack equal to $\alpha = 27.5^\circ$ (this case representing high angles of attack, close to the stall angle) are

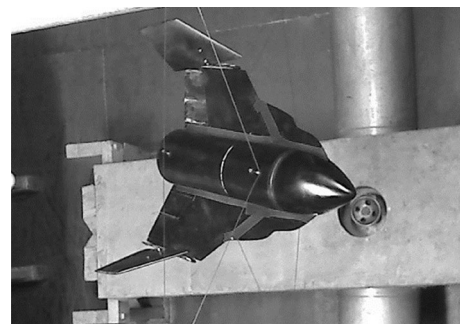
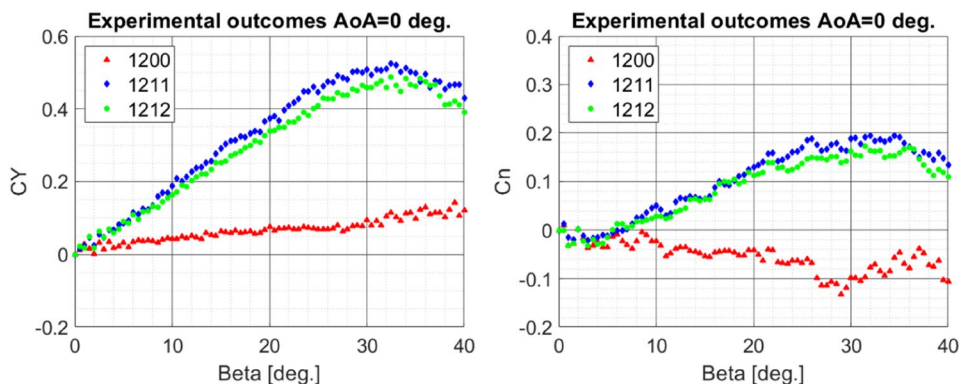


Fig. 11 Top view of model 1212 with the all moving tail deflected under the direction test

Fig. 12 Side force coefficient (on the left) and yaw moment coefficient (on the right) versus the sideslip angle for the angle of attack equal to $\alpha = 0^\circ$



presented in Fig. 13. According to the assumed sign convention of the yawing moment (see Fig. 10), the aircraft is statically directionally stable, if the yawing moment coefficient curve has a positive slope [26]. It means that the condition (1) must be fulfilled.

$$\frac{\partial C_n}{\partial \beta} > 0 \tag{1}$$

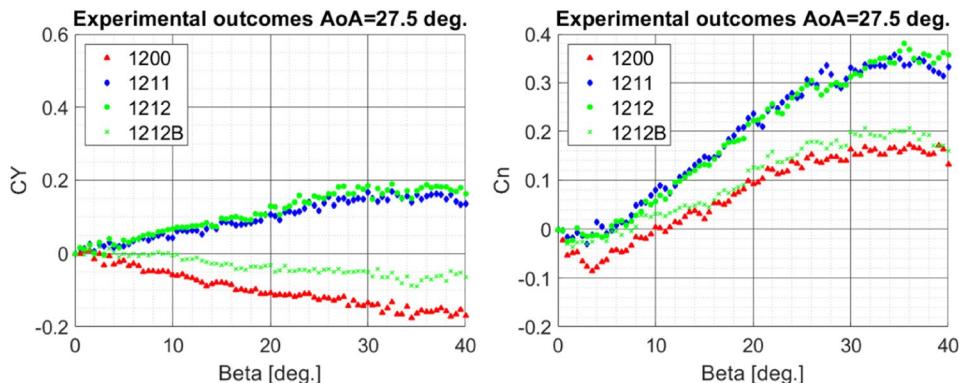
All force and moment coefficients were referred to the same reference values, as the reference length the rocket plane wingspan without the side plates was assumed. For all considered configurations of the side plates, a small instability ($\frac{\partial C_n}{\partial \beta} < 0$) was observed for low sideslip angles ($\beta = 0^\circ$ to $\beta = 5^\circ$). This phenomenon was observed for both low and high angles of attack (Figs. 12 and 13). After that the rocket plane is directionally statically stable up to the sideslip angle of $\beta = 32^\circ$. The effect of the configuration of side plates on the directional static stability is relatively small when the angle of attack is high. While for the low angles of attack the slope for model 1211 is steeper which means that this configuration is more directional stable. The angle of the bottom plate of the configuration 1212 is equal to $\Theta_d = 0$ (it's parallel to x-z plane) which means that the projection area of low plate is going to be bigger than for 1211 configuration. This would indicate that the geometry of the upper plate has a

bigger impact on the directional stability (slope) for low angles of attack than the lower plate. This was also confirmed by numerical results computed by MGAERO, the numerical results are presented in numerical outcomes.

4.2 Directional aerodynamic characteristics for the deflected all moving tail

The tests for model with control surfaces deflected were carried out again for two angles of attack. For $\alpha = 0^\circ$ which represents the case for a small angle of attack and $\alpha = 27.5^\circ$ (the value just before the critical angle of attack). In this part of the investigation, only model 1212 with all moving tail deflected was tested. Two types of all moving tail deflection were tested, the first one was a symmetrical deflection when both side plates were deflected as it is presented in Fig. 14. The second type was asymmetrical deflection when only a single plate was deflected while the second plate is in the neutral position. In case of the asymmetrical deflection, four possible configurations can occur, see Fig. 15. Each of those configurations generate different side force and yaw moment. This is caused by the different local angle of attack on each side plates. If the side plate deflection is like on Fig. 15B or D, then the local angle of attack on this deflected side plate is reduced ultimately making lower side force for the low side slip angles. While for the high slip angles can generate more side force than

Fig. 13 Side force coefficient (on the left) and yaw moment coefficient (on the right) versus the sideslip angle for the angle of attack equal to $\alpha = 27.5^\circ$



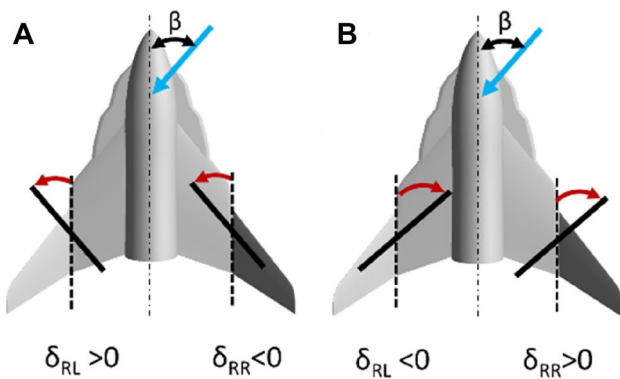


Fig. 14 Possible of symmetrical deflections

the configuration with opposite type of deflection like Fig. 15A or Fig. 15C. Where for those configurations the local angle of attack is bigger for the low side slip angles but earlier the force decreased due to exceeding the stall angle. In case of the yaw moment, it is the net effect of the side force and drag which is also related to the local angle of attack. Moreover, deflection as presented in Fig. 15B is not going to give the same force as configuration presented

in Fig. 15D because the flow around left side plate is affected by the fuselage. Firstly, the results for symmetrical side plates deflection are presented. The plots of the yawing moment coefficient and side force coefficient versus the sideslip angle, for the case of the angle of attack equal to $\alpha=0^\circ$ are presented in Fig. 16. The model is statically directionally stable up to the sideslip angle of about $\beta=32^\circ$. The plots of the yawing moment coefficient and side force coefficient versus the sideslip angle for model 1212 with all moving tail deflected, for the angle of attack equal to $\alpha=27.5^\circ$ are presented in Fig. 17. The model is directionally statically stable for sideslip angles from 5° to 35° . The difference in the side force and yaw moment between different deflection is caused by the earlier mentioned issue with a local angle of attack.

Using MGAERO software, the investigation into the flow structure was conducted. The flow visualization is presented in Fig. 18, it can be observed that two vortices are generated from the LEX and moving along the rocket plane until the end of the vehicle. Those vortices are located inside (between the fuselage and inner part of the upper side plate). Also, there can be observe one vortex which is outside of the side plate, which affecting the flow

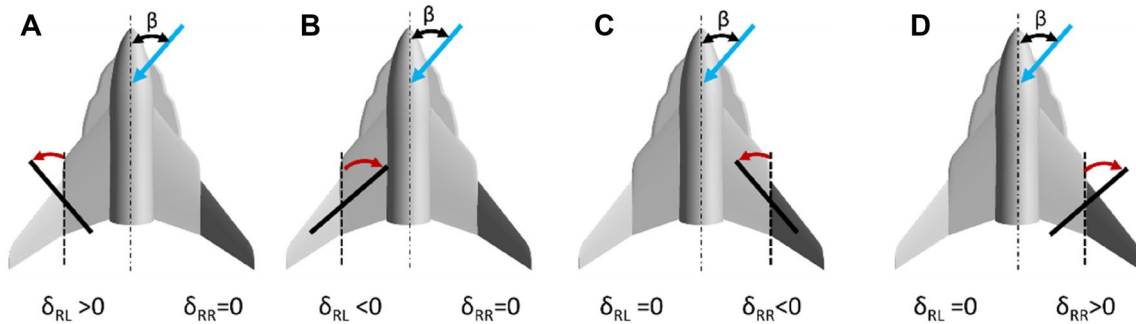


Fig. 15 Possible of asymmetrical deflections

Fig. 16 Side force coefficient (on the left) and yaw moment coefficient (on the right) versus the sideslip angle for the angle of attack equal to $\alpha=0^\circ$ all moving tail symmetrical deflection

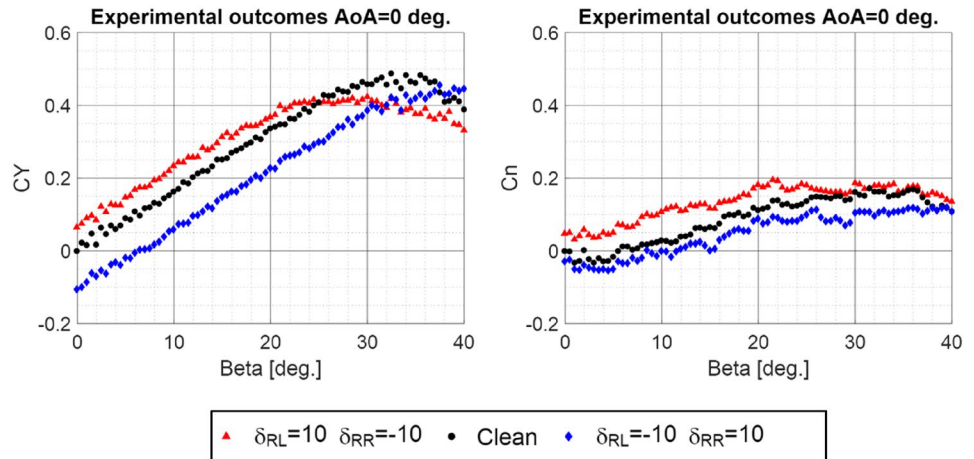


Fig. 17 Side force coefficient (on the left) and yaw moment coefficient (on the right) versus the sideslip angle for the angle of attack equal to $\alpha=27.5^\circ$ - all moving tail symmetrical deflection

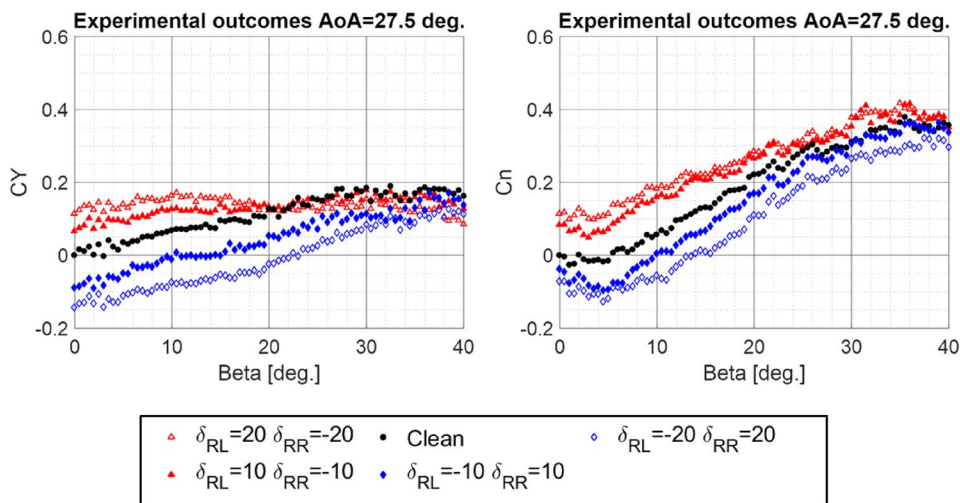
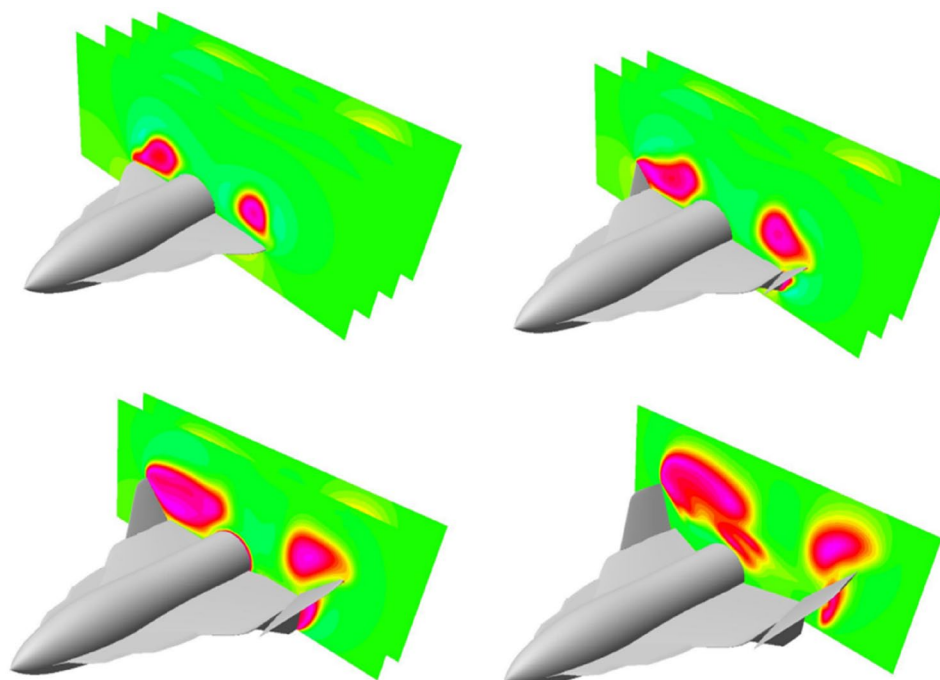


Fig. 18 Example of the flow visualization for $\alpha=27.5^\circ$ and $\beta=10^\circ$, in case of deflection of $\delta_{RL}=10$ and $\delta_{RR}=-10$



around the bottom left plate, and causing that it generates bigger side force than the right bottom plate.

Also forces and moments for the asymmetrical deflection (only one plate is deflected, possible deflections are presented in Fig. 15) of all moving tail were measured. As it was expected, the asymmetrical deflection shows lower effectiveness in comparison to the symmetrical case, but this can be observed only up to $\beta=25$ deg. The different values of the side force and yawing moment coefficients were observed for two opposite cases of asymmetrical deflection (see Fig. 19). For low and very high sideslip angles, the side force is different when deflected was only the left side plate ($\delta_{RL}=10$ and $\delta_{RR}=0$) in comparison to the case when

only the right-side plate was deflected ($\delta_{RL}=0$ and $\delta_{RR}=10$ see Fig. 19). This is caused by a different effective angle of attack on the side plate which depends on the position of the deflected plates in respect to the free stream velocity and the cross flow that occurs due to the sideslip angle. The same phenomenon does occur for symmetrical side plates deflection.

Using MGAERO software, the investigation into a flow structure for the asymmetrical deflection was conducted. The flow visualization for two different cases was presented in Fig. 20 and Fig. 21. But the simulation set-up is the same for all presented cases and correspond to $Ma=0.1$, $\alpha=27.5$ deg. and $\beta=20$ deg. In case of Fig. 20, in both presented cases,

Fig. 19 Side force coefficient (on the left) and yaw moment coefficient (on the right) versus the sideslip angle for the angle of attack equal to $\alpha=0^\circ$ - all moving tail asymmetrical deflection

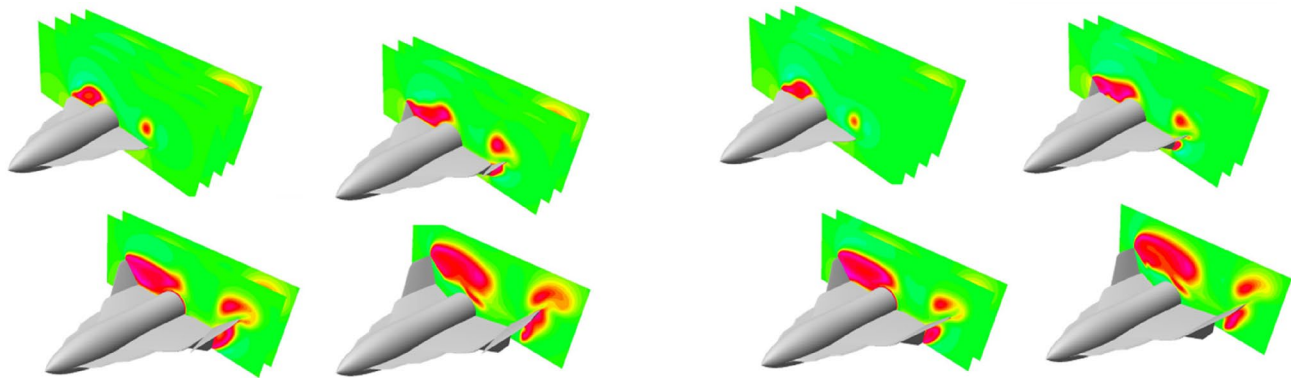
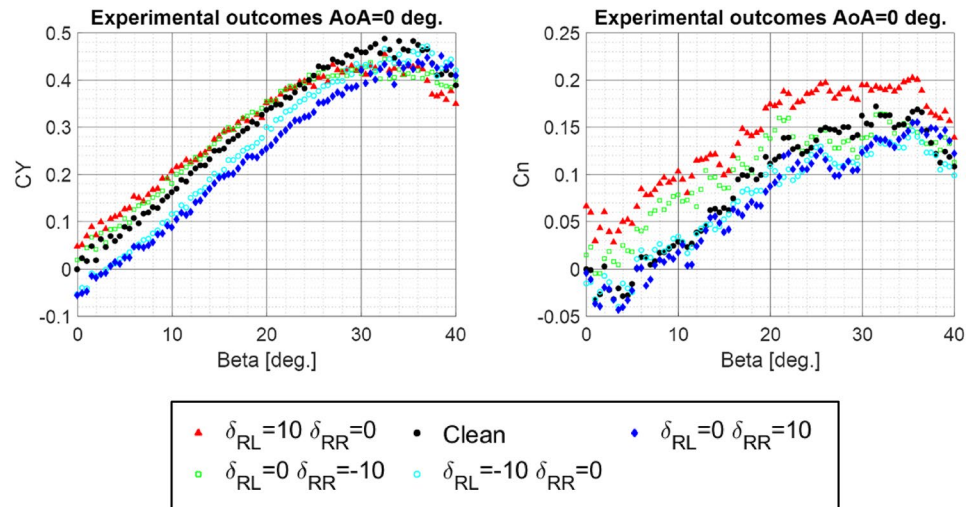
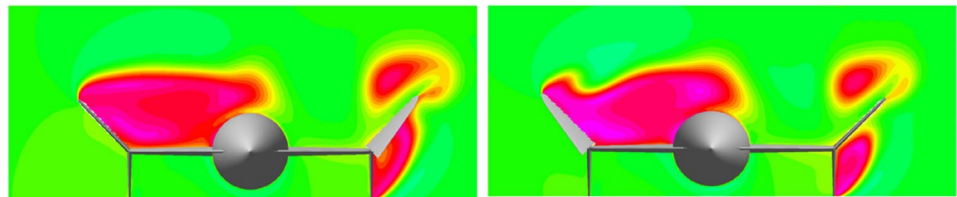


Fig. 20 Example of the flow visualization for $\alpha=27.5^\circ$ and $\beta=20^\circ$, in case of deflection of $\delta_{RL}=10$ and $\delta_{RR}=0$ (set off pictures on the left) and $\delta_{RL}=0$ and $\delta_{RR}=10$ (set off pictures on the left)

Fig. 21 Example of the flow visualization for $\alpha=27.5^\circ$ and Beta $\beta=20^\circ$, in case of deflection of $\delta_{RL}=10$ and $\delta_{RR}=0$ (set off pictures on the left) and $\delta_{RL}=0$ and $\delta_{RR}=10$ (set off pictures on the left)



the side plates are deflected in the same direction (with respect to the free stream flow), but on the left set of picture it is the left side plate while on the right side set of picture it is the right plate. Also in case of the deflection of opposite side plates, in opposite direction is consider like in Fig. 21. The structure of the flow is very similar which agree with the data measured in the wind tunnel, there is a slight difference. For left upper side plate, in case of the configuration with deflected left side plate, the vortex around this plate is stronger (Fig. 21).

Moreover, the impact of the side plate deflection on C_D , C_L and C_{MY} was analyzed using the numerical data. The

most significant difference was observed for drag coefficient while the change of the lift coefficient is the less visible (Fig. 22).

The influence of the all moving tail on stability and control characteristics were analyzed. The plots of the all moving tail's side force versus the sideslip angles and all moving tail's side force derivatives with respect to the sideslip angle versus the sideslip angle are presented in Fig. 23. The slope of the side force is bigger for case of low angles of attack ($\alpha=0^\circ$). The effectiveness of the yaw control was done based on the average value of the derivative of the side plate force with respect to the angle of the all moving

Fig. 22 Impact of asymmetrical deflection on longitudinal characteristics, results obtained by MGAERO software

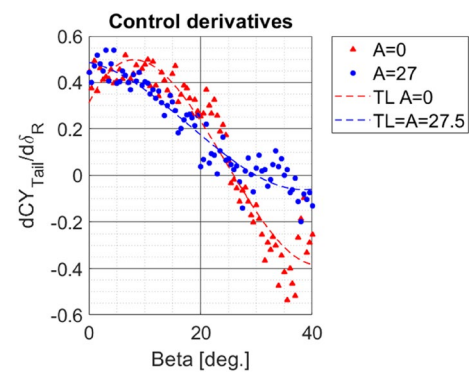
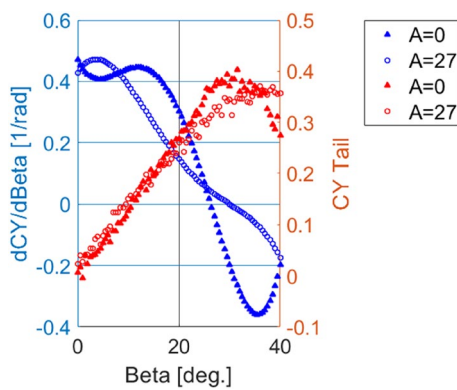
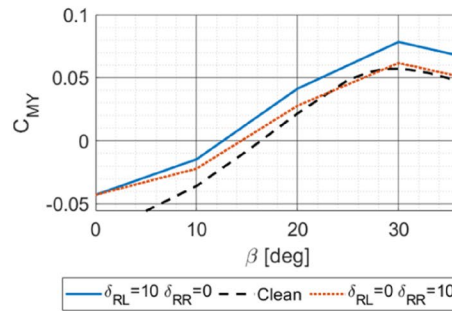
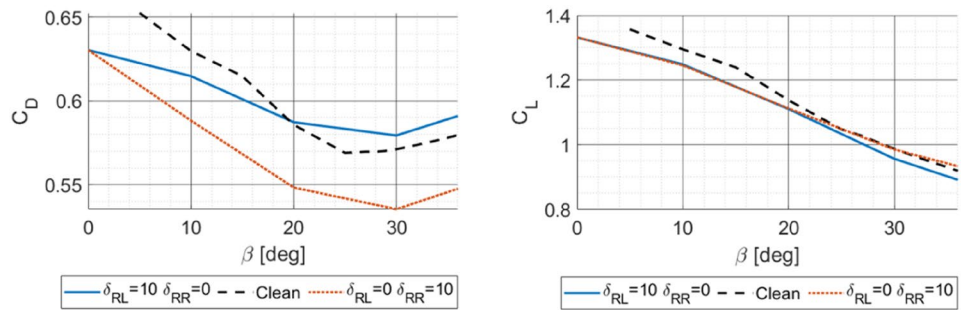


Fig. 23 Side plate's force versus the sideslip angle and side plate's force derivative with respect to the sideslip angle versus the sideslip angle

Fig. 24 Side plate's force derivative with respect to the all moving tail deflection angle versus the sideslip angle

tail deflection. Figure 24 shows the plot of this derivative versus the sideslip angle when the angles of attack is equal to $\alpha=0^\circ$ and $\alpha=27.5^\circ$. In case of the low sideslip angle the effectiveness of the all moving tail is higher for $\alpha=0^\circ$, while for higher sideslip angle the inversion of control derivatives can be observed. This inversion occurs earlier for the case of $\alpha=0^\circ$ and latter for $\alpha=27.5^\circ$.

$\alpha=27.5^\circ$, $\beta=20^\circ$, and $V=20$ m/s. That method of flow visualization on the aircraft surface was used mainly to check the vortex flow caused by the LEX. Moreover, the visualization revealed that for high angles of attack the upper plates generate a pair of vortices which was also confirmed by the numerical simulation.

4.3 Oil visualization

4.4 Numerical outcomes

The last part of the wind tunnel experiment consisted in an oil visualization. Figure 25 presents the directional case for:

The last part of the comparison between the experimental and numerical results are outcomes for low AoA. The numerical computations were done for both 1211 and 1212



Fig. 25 Oil visualization for model 1212 $\alpha=27.5^\circ$, $\beta=20^\circ$, and $V=20$ m/s

rocket plane configurations. The aim for this comparison was to determine if software that using a simple flow model can be useful for an initial design (low angles of attack) of the aircraft with side-plate working as all moving tail.

Figures 26 and 27 are presenting the comparison of coefficient of side force and yawing moment versus sideslip angle obtained by the numerical software and measured in the wind tunnel. The side force slope can be predicted with reasonable accuracy (Table 2) while the yaw moment due to nonlinear character is not well predicted by the potential flow (PANUKL).

Fig. 26 Comparison of the numerical and experimental results for model L1211

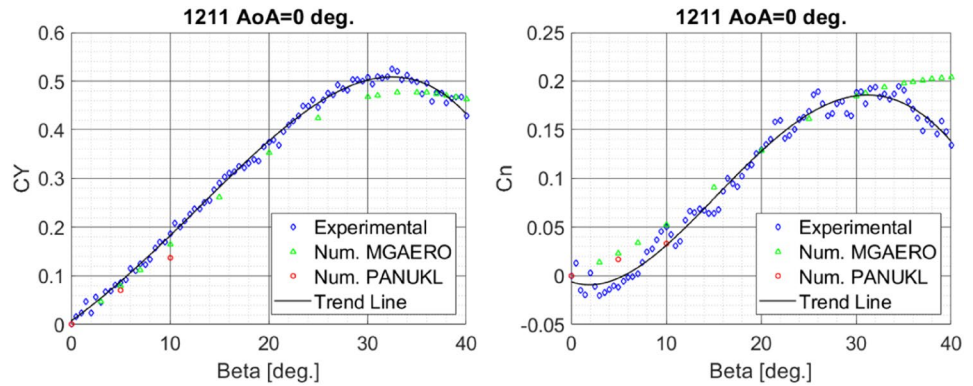


Fig. 27 Comparison of the numerical and experimental results for model L1212

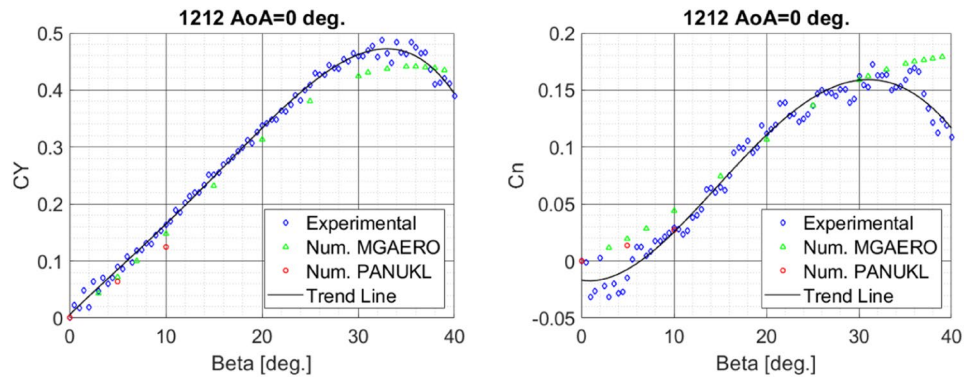


Table 2 Comparison of the dimensionless derivatives for both numerical and experimental cases, for $\alpha=0^\circ$

Conf. 1212	Exp	MGAERO	PANUKL
$\frac{\partial C_Y}{\partial \beta}$	-0.905	-0.647	-0.718
$\frac{\partial C_n}{\partial \beta}$	0.467	0.465	0.156
Conf. 1211	Exp	MGAERO	PANUKL
$\frac{\partial C_Y}{\partial \beta}$	-1.008	-0.812	-0.789
$\frac{\partial C_n}{\partial \beta}$	0.517	0.524	0.190

5 Conclusions

The research outcomes which were presented above, concentrated on analysis of the directional static stability and control of the rocket plane in the tailless configuration. The study was conducted based on data measured in the low-speed wind tunnel and numerical computations. During the experiment, two sets of side plates were examined and a model with deflected side plates as the all moving tail was analyzed.

The geometry and configuration of the side plates for all the considered models exert a relatively little effect on directional static stability for high angles of attack. While for high angles of attack the yaw angle of the upper side plate has an impact on the side force slope. This can be concluded that the impact of the bottom plate's geometry on the directional static stability for low angles of attack is negligible.

For all considered configurations of the side plates small instability ($\frac{\partial C_n}{\partial \beta} < 0$) was observed for low sideslip angles ($\beta = 0^\circ$ to $\beta = 5^\circ$). This phenomenon was observed for both low and high angles of attack (Fig. 13 and Fig. 14). Because the numerical computations do not show such a behavior (Fig. 26 and Fig. 27) this issue could be caused by the manufacture imperfection of the rocket plane model as well as by the technique how the model is mounted in the wind tunnel. This ultimately might cause occurrence of unplanned an asymmetrical flow. Also due to relatively low forces that are recorded for low sideslip angles as well as the sensor sensitive to vibration that might also affect the wind tunnel balance readings.

The effectiveness of control surfaces was examined only for all moving tail configuration 1212. This was evaluated by the calculation of the control derivatives of the all moving tail side force with respect to the sideslip angle as well as the all moving tail side force with respect to the all moving tail angle of deflection. For a medium sideslip angle (up to the 27°) the derivatives are larger than for the low angle of attack ($\alpha = 0^\circ$). The effectiveness of control surfaces for the high angle of attack ($\alpha = 27.5^\circ$) is higher than for higher sideslip angles. For a sideslip angle exceed $\beta = 26^\circ$ the inversion of control derivatives was observed for $\alpha = 0^\circ$, while the inversion for $\alpha = 27.5^\circ$ occurred later, about $\beta = 30^\circ$. Probably it was caused by the position of a vortex relative to the all moving tail and bigger drag.

The all moving tail asymmetrical deflection allows for decreasing the side force and yawing moment for low and moderate side slip angles but for $\beta > 25$ is more effective than the symmetrical deflection. This is caused by the distribution of the local angle of attack on the side plates.

Base on comparison of the numerical and experimental results can be concluded that the side force slope can be predicted with reasonable accuracy even using a simple flow

model as potential flow. However, the yaw moment due to nonlinear character is not well predicted by the potential flow.

Acknowledgements The authors would like to express their gratitude to Warsaw University of Technology students: P. Falczyński and M. Milewska for taking part in the wind tunnel tests as a part of their bachelor theses.

Funding No funding was received to assist with the preparation of this manuscript.

Declarations

Conflict of interests The authors have no relevant financial or non-financial interests to disclose.

Open Access This article is licensed under a Creative Commons Attribution 4.0 International License, which permits use, sharing, adaptation, distribution and reproduction in any medium or format, as long as you give appropriate credit to the original author(s) and the source, provide a link to the Creative Commons licence, and indicate if changes were made. The images or other third party material in this article are included in the article's Creative Commons licence, unless indicated otherwise in a credit line to the material. If material is not included in the article's Creative Commons licence and your intended use is not permitted by statutory regulation or exceeds the permitted use, you will need to obtain permission directly from the copyright holder. To view a copy of this licence, visit <http://creativecommons.org/licenses/by/4.0/>.

References

1. The Tauri Group: Suborbital Reusable Vehicles: A 10-Year Forecast of Market Demand, https://brycetech.com/reports/report-documents/FAA_SRV_2012.pdf, (Accessed 22.12.2021)
2. Great Expectations: An Assessment of the Potential for Suborbital Transportation, International Space University, Final Report of Masters Program 2007–2008 of the International Space University in Strasbourg, France, https://isulibrary.isunet.edu/doc_num.php?explnum_id=95, (Accessed 22.12.2021)
3. Di Benedetto, S., Di Donato, M.P., Schettino, A., et al.: The high-speed experimental flight test vehicle of HEXAFly-INT: a multidisciplinary design. *CEAS Space J.* **13**, 291–316 (2021). <https://doi.org/10.1007/s12567-020-00341-5>
4. Krummen, S., Sippel, M.: Effects of the rotational vehicle dynamics on the ascent flight trajectory of the SpaceLiner concept. *CEAS Space J.* **11**, 161–172 (2019). <https://doi.org/10.1007/s12567-018-0223-7>
5. Gonçalves, P.M., Lino da Silva, M., dos Reis, R.J.N., et al.: Hypersonic transatmospheric and exoatmospheric vehicle design using the SUAVE tool. *CEAS Space J.* **12**, 171–190 (2020). <https://doi.org/10.1007/s12567-019-00283-7>
6. Yi-Wei, C., Jeng-Shing, C.: A preliminary study on the potential spaceports for suborbital space tourism and intercontinental point-to-point transportation in Taiwan. *Acta Astronaut.* **181**, 492–502 (2021). <https://doi.org/10.1016/j.actaastro.2020.11.059>
7. Galiński, C., Goetzendorf-Grabowski, T., Mieszalski, D., Stefanek, Ł.: A concept of two-staged spaceplane for suborbital tourism. *Trans. Inst. Aviat.* **191**(4/2007), 33–42 (2007)

8. Figat, M., Galiński, C., Kwiek, A. 2012 Modular Aeroplane System. A Concept and Initial Investigation, Proceedings of the 28th Congress of the International Council of the Aeronautical Sciences, 23-28.09.2012 Brisbane, Paper No ICAS 2012-1.3.2, ISBN 978-0-9565333-1-9
9. Evans, R., A., Bloor, M., I., G. 1980 Strake/Delta Wing Interactions at High Angles of Attack, NASA- Contractor Report 166183, available at <https://ntrs.nasa.gov/api/citations/19810017536/downloads/19810017536.pdf>, (Accessed 23.08.2022)
10. Lamar J. E., Frink N., T. 1981 Experimental and Analytical Study of the Longitudinal Aerodynamic Characteristics of Analytically and Empirically Designed Strake-Wing Configurations at Subcritical Speeds, NASA Technical Paper 1803, Hampton, Virginia, available at <https://ntrs.nasa.gov/api/citations/19810016505/downloads/19810016505.pdf>, (Accessed 23.08.2022)
11. Figat, M., Kwiek, A.: Aerodynamic and static stability investigation into aircraft coupled system to suborbital space flights. *Aircr. Eng. Aerosp. Technol.* **93**(2), 275–283 (2021)
12. Figat, M., Kwiek, A.: Aerodynamic optimisation of the rocket plane in subsonic and supersonic flight conditions. *Proc. Inst. Mec. Eng. Part G J. Aerosp. Eng.* **231**(12), 2266–2281 (2017)
13. Kwiek, A. 2014 Study on control and stability of the rocket plane to space tourism, Proceedings of the 29th Congress of the International Council of the Aeronautical Sciences, 7-12.09.2014 St. Petersburg Russia, Paper No ICAS2014_0893, ISBN: 3-932182-80-4
14. Kwiek, A., Galinski, C., Bogdanński, K., Hajduk, J., Tarnowski, A.: Results of simulation and scaled flight tests performed on a rocket-plane at high angles of attack. *Aircr. Eng. Aerosp. Technol.* **93**(9), 1445–1459 (2021)
15. Kwiek, A., Figat, M.: LEX and wing tip plates interaction on the Rocket Plane in tailless configuration. *Aeronaut. J.* **120**(1224), 255–270 (2016)
16. Schettino, A., Pezzella, G., Marini, M., et al.: Aerodynamic database of the HEXAFLY-INT hypersonic glider. *CEAS Space J.* **12**, 295–311 (2020). <https://doi.org/10.1007/s12567-020-00299-4>
17. Grantz, A. C. 1984 The Lateral-Directional Characteristics of a 74 degree Delta Wing Employing Gothic Planform Vortex Flaps., NASA Contractor Report 3848, available at <https://ntrs.nasa.gov/api/citations/19850003701/downloads/19850003701.pdf>, (Accessed 23.08.2022)
18. Erickson, G. E. 2007 Wind Tunnel Investigation of the Effects of Surface Porosity and Vertical Tail Placement on Slender Wing Vortex Flow Aerodynamics at Supersonic Speeds, NASA Technical Memorandum 2007-215082, available at <https://ntrs.nasa.gov/api/citations/20070034019/downloads/20070034019.pdf>, (Accessed 23.08.2022)
19. Analytical Methods, INC., MGAERO user's manual Version 3.1.4, Redmond, Washington USA, 1990-2001
20. Mavriplis, D.J.: Three-dimensional unstructured multigrid for the Euler equations. *J. Aircr.* **30**(7), 1753–1761 (1992)
21. Cummings, R.M., Forsythe, J.R., Morton, S.A., Squires, K.D.: Computational challenges in high angle of attack flow prediction. *Prog. Aerosp. Sci.* **39**(5), 369–384 (2003)
22. PANUKL potential solver, Software package, Warsaw University of Technology, <https://www.meil.pw.edu.pl/add/ADD/Teaching/Software/PANUKL>
23. Goetzendorf-Grabowski, T., Tarnowski, A., Figat, M., Mieloszyk, J., Hernik, B.: Lightweight unmanned aerial vehicle for emergency medical service – synthesis of the layout. *Proc. Inst. Mec. Eng. Part G J. Aerosp. Eng.* **235**(1), 5–21 (2021)
24. Mieloszyk, J., Tarnowski, A., Tomaszewski, A., Goetzendorf-Grabowski, T.: Validation of flight dynamic stability optimization constraints with flight tests. *Aerosp. Sci. Technol.* **106**, 106193 (2020)
25. Luckring J.M. 2004 Reynolds Number, compressibility, and leading-edge bluntness effects on Delta-Wing Aerodynamics”, Proceedings of 24th International Congress of the Aeronautical Sciences 2004 29.08–03.09 2004, Yokohama, Japan Paper No ICAS 2004-4.1.4
26. Nelson R. C.: Flight Stability and Automatic Control, 2nd ed., WCB McGraw-Hill, Boston (1998)
27. Witoszyński C.: Travaux de L'Institut Aerodynamique de Varsovie. Fascicule V, Warsaw 1932, http://bcpw.bg.pw.edu.pl/dlibra/docmetadata?id=3157&from=&dirids=1&ver_id=49254&lp=4&QI=!EFCF9417B69770894E5914376646D2BD-59 a document in Polish and French, (Accessed 22.12.2021)

Publisher's Note Springer Nature remains neutral with regard to jurisdictional claims in published maps and institutional affiliations.